Geochronology, 8, 279–295, 2026
https://doi.org/10.5194/gchron-8-279-2026

^{40}Ar / ^{39}Ar constraints on the eruption history of the Christiana Volcano of the Christiana-Santorini-Kolumbo volcanic field, Greece

Pieter Z. Vroon[1], Teun Beemster[1], Xiaolong Zhou[1], Paraskevi Nomikou[2], Martijn Klaver[1], Jan R. Wijbrans[1], and Klaudia F. Kuiper[1]

[1]Department of Earth Sciences, Faculty of Science, VU University Amsterdam, De Boelelaan 1085, 1081 HV Amsterdam, the Netherlands
[2]National and Kapodistrian University of Athens, Department of Geology and Geoenvironment, Panepistimioupoli Zografou, 15784 Athens, Greece

Correspondence: Pieter Z. Vroon (p.z.vroon@vu.nl)

Received: 1 October 2025 – Discussion started: 22 October 2025
Revised: 22 January 2026 – Accepted: 5 February 2026 – Published: 27 May 2026

Abstract. The Christiana Islands group consists of three at present uninhabited islands 20 km SW of Santorini, Aegean Sea, Greece, that are the subaerial remnants of the Christiana volcano. The age of the Christiana Islands has been unclear and has been previously assumed to have started around the same time as the emergence of Santorini (600 ka). Other studies, based on seismic reflection, have correlated volcanic deposits of the Christiana archipelago to Pliocene sedimentary layers. Five subaerial Christiana volcanic rocks of the Upper Lava formation cluster tightly between 2.57–2.69 Ma with relatively small uncertainties (0.02–0.03 Ma). One sample dated much younger: 133 ka; this obsidian from a pyroclastic deposit is most likely derived from the Middle Pumice Plinian eruption of Santorini. The 2.5–2.7 Ma age for Christiana volcano shows that all volcanic fields of the South Aegean Volcanic Arc (SAVA) were active around 3 Ma ago and started when oceanic crust arrived at 100 km depth below the SAVA volcanic fields after a long period of continental lithosphere subduction. The Christiana volcano was constructed when the local stress field showed NNE-SSW extension. During the transition from NNE-SSW to NW-SE extension the Christiana volcano became extinct and a period of > 1.0 Ma with volcanic quiescence and/or low volcanic output followed until the start of submarine volcano Poseidon and present-day volcanic centres Santorini and Kolumbo.

1 Introduction

Although the Christiana Archipelago is part of the Christiana-Santorini-Kolumbo volcanic field (CSK-VF), which contains with Santorini probably one of the best studied volcanoes worldwide (e.g. Druitt et al., 1999), the Christiana islands have not received the same level of attention. Only two papers have been published in the last 50 years (Puchelt et al., 1977; Aarburg and Frechen, 1999). The Christiana islands have been presumed to be geologically similar to the older lavas from the Akrotiri peninsula of Santorini with an age of approximately 600 ka, (e.g. Francalanci et al., 2005). However, other studies have suggested that submarine deposits from Christiana interfinger with Pliocene-Early Pleistocene sediments in seismic studies (Piper et al., 2007). Based on sedimentation rates of 10 cm ka^{-1} this would result in approximate ages of ~ 1.7 Ma (Piper et al., 2007) and ~ 1.6 Ma (Preine et al., 2021). The last study also mentioned that volcanism probably lasted several hundred thousand years. Given the uncertainty of the sedimentation rates and interpretation of seismic profiles, the aim of this study is to obtain for the first time high resolution isotopic ages from the subaerial volcanics of the Christiana Archipelago and discuss the temporal evolution of the CSK-VF based on these results.

2 Gelogical background

2.1 The South Aegean Volcanic Arc (SAVA)

The Christiana-Santorini-Kolumbo volcanic field (CSK-VF) is located in the central section of the South Aegean Volcanic Arc (SAVA) which consists of five principal volcanic fields: Sousaki (or Crommyonia, S-VF), Aegina-Poros-Methana (APM-VF), Milos (M-VF), Christiana-Santorini-Kolumbo and Kos-Nisyros-Yali (KNY-VF) (Vougioukalakis et al., 2019) (Fig. 1A). The SAVA is the result of northward subduction of the African plate underneath the Eurasian plate at the Hellenic trench system that is located south of Crete (see Fig. 1A). Tomographic studies show that an approximately 1500 km long African slab has subducted (e.g. Spakman et al., 1988; Ring et al., 2010), which suggests that subduction started in the Jurassic (Van Hinsbergen et al., 2014). Multiple continental terranes have been accreted to the Eurasian plate during subduction related convergence, and this resulted in the formation of a stacked complex of thrust sheets of mainly continental affinity, called the Hellenides Complex (e.g. Jolivet and Brun, 2010; Van Hinsbergen et al., 2014). The current accretionary wedge, at present located on and to the south of Crete, will be the last continental terrane to accrete to this Hellenides complex, after which a continent-continent collision between south-eastern Eurasia and the thinned margin of Africa will commence (Le Pichon et al., 2002).

Fragmentation of the African slab due to tearing beneath Italy (Jolivet et al., 2013) and subduction lock near Cyprus (Brun and Sokoutis, 2010) caused upwelling of enriched mantle material through assumed gaps in the fragmented slabs (e.g. Boehm et al., 2023; Klaver et al., 2016), but there is discussion how this affects Aegean Arc magmatism (e.g. Ersoy and Palmer, 2013; Klaver et al., 2016). Slab roll-back caused extension in the Aegean domain and as a result the continental crust underneath the CSK-VF is currently approximately 25 km thick (see Fig. 1A). Slab roll-back is also responsible for the southward migration of the volcanic arc, and the SAVA was formed at its present-day location approximately 5 Ma ago (e.g. Vougioukalakis et al., 2019). The location of volcanoes in the different VFs is strongly controlled by the extensional tectonic regime as suggested for Methana-Poros (e.g. Pe-Piper and Piper, 2013; Elburg et al., 2018), Milos (Zhou et al., 2021), Santorini (e.g. Heath et al., 2019; Preine et al., 2022a) and Nisyros (e.g. Nomikou et al., 2013).

The Sousaki VF can be separated in an older western part (4.1–3.6 Ma) and younger eastern part (2.7–2.3 Ma). Both parts consist of small ($< 1\ km^3$) dacitic lava domes and flows (Vougioukalakis et al., 2019). The oldest submarine volcanism of the APM VF is recorded on Aegina between 4.7 and 4.3 Ma. The main phase of subaerial volcanism on Aegina occurred between 3.9–3.0 Ma with the extrusion of lava domes and flows (Vougioukalakis et al., 2019). Between 3.0–2.1 Ma there was a period of low volcanic output, followed by a period of 0.1 Ma with the extrusion of basaltic andesitic to andesitc subaerial lava. During the Pleistocene there was some volcanic output, but for the last 0.7 Ma Aegina was not active (Vougioukalakis et al., 2019). Poros is characterised by one lava dome with an age of 3.1–2.6 Ma (Vougioukalakis et al., 2019). Methana has been active from 3.6 Ma to historic times without major hiatuses and volcanic products are characterised by dacitic-andesitic lava domes and block-and-ash flows. The hornblende-dacites and pyroxene-andesites on Methana and porphyritic dacites and andesites on Aegina are comparable to those found on Christiana.

The Milos VF has been active from ~ 3.3 Ma onwards (e.g. Zhou et al., 2021) and consists of the Milos, Kimolos, Polygos, Antimilos islands and the Ananes islets (Vougioukalakis et al., 2019). This VF is composed of many small eruption points that mostly produced andesitic to rhyolitic pumice cones and lava domes. The only composite volcano of this VF is Antimilos. Volcanism on the island of Milos can be subdivided in three periods: period I (3.3–2.13 Ma) and III (1.6–0 Ma) with low magma fluxes and period II (2.13–1.6 Ma) with a higher volcanic output (Zhou et al., 2021). Volcanic products of Polygos and Kimolos have ages that overlap with Period I, whereas available age data for Antimilos overlaps with Period III (0.38 Ma).

The KNY-VF consist of volcanic deposits that are found on SW Kos, the composite volcano Nisyros and an uplifted submarine pumice cone and obsidian dome that now form Yali. The southern part of Kos contains dacite stocks and rhyolite domes which range in age from 2.6–0.5 Ma (Bachmann et al., 2010). The lower part of the islet of Pyrgousa is composed of andesitic domes that represent a remnant of the volcanic edifice and has probably a maximum K-Ar age ~ 1.9 Ma with additional uncertainty added due to the suspected presence of excess ^{40}Ar (Piper et al., 2019). Around 0.5 Ma the Kefalos tuff cone built up and a small caldera was also created (Vougioukalakis et al., 2019). The next event was the large caldera forming eruption at 161 ka (Allen, 2001) that deposited the Kos plateau tuff (KPT).

The stratovolcano Nisyros is significantly younger than Christiana and formed after the KPT eruption (< 160 ka, Dietrich and Lagios, 2017). The young volcanics of both Nisyros and Yali have proven to be very difficult to date, but Popa et al. (2020) dated the felsic products of Nisyros and Yali using Th-U disequilibrium of zircon crystals and obtained minimum ages between 120 to 20 ka and 40 to 23 ka, respectively.

2.2 The Christiana-Santorini-Kolumbo volcanic field (CSK-VF)

The Christiana-Santorini-Kolumbo volcanic field (CSK-VF) consists of the Christiana Archipelago in the southwest, the Santorini Archipelago in the centre and the Kolumbo seamount chain towards the northeast of Santorini (Fig. 1B). These volcanoes are on a straight NE-SW trend referred to

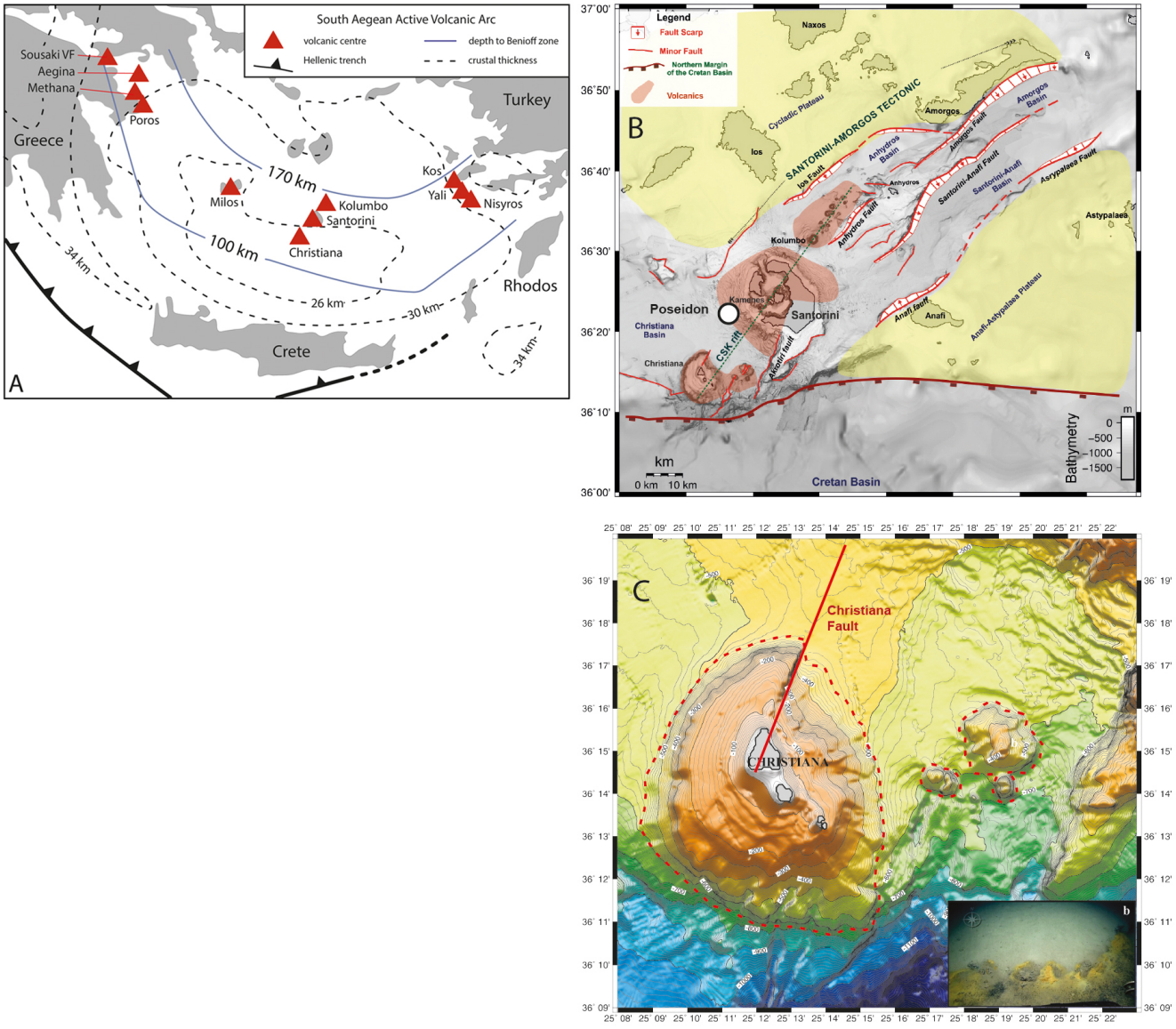

Figure 1. **(A)** Overview of the Aegean arc with the main volcanic fields (after Klaver, 2016). **(B)** Overview of the Christiana–Santorini–Kolumbo volcanic field (from Nomikou et al., 2013). **(C)** Swath bathymetric map of Christiana volcano with 10 m isobaths (after Nomikou et al., 2013).

as the Christiana-Santorini-Kolumbo (CSK) tectonic line located in a rift zone of 60 km between the Cycladic and the Anafi-Astipalaea Plateaus (e.g. Nomikou et al., 2019). A detailed summary of the tectonic and volcanic evolution of the CSK-VF is given by Metcalfe et al. (2025). The Kolumbo seamount chain consists of 26 small submarine cones and the larger Kolumbo seamount running along the CSK tectonic line (see Fig. 1B). The Kolumbo seamount is a submarine volcano with a diameter of 1700 m which has a centre crater with the crater floor at 500 m depth (Nomikou et al., 2013). The Kolumbo volcano is composed of 5 sub-circular units (K1–K5) that are derived from different volcanic eruptions (Hübscher et al., 2015). Unit K5 is from the last eruption of 1650 AD, whereas unit K1–K2 are thought to be significantly older based on seismic imaging and sedimentation rates: ∼ 1.2 Ma (Preine et al., 2021). Unit K3 probably correlates with the older phases of Santorini (∼ 0.5 Ma) (Preine et al., 2021). Klaver et al. (2016) studied the geochemical composition of the Kolumbo volcanics and concluded that the Santorini and Kolumbo volcanoes tap distinct mantle sources.

The Santorini volcano is composed of a submerged caldera of 10 by 7 km that is surrounded by three islands, Thera, the main island, with Therasia and Aspronisi forming the remnants of the western flank of the volcanic centre. Inside the caldera are two small islands Palea- and Nea Ka-

meni that consist of eruptive centres that have formed after the last large Late Bronze Age (LBA) explosive eruption of ~ 3600 BP (e.g. Druitt et al., 2019). The exposed lithologies on Santorini include a metamorphosed schist-marble series similar to the rocks found in the Cycladic massif to the north. Metamorphic rocks are also found as lithic fragments incorporated in volcanic products (e.g. Druitt et al., 1999).

The oldest subaerial volcanic products of Santorini are amphibole bearing lavas on the Akrotiri Peninsula with an age of 650–550 ka. Recent IODP drilling discovered a giant offshore pumice deposits called the Archaeos Tuff in the basins surrounding Santorini (Druitt et al., 2024). The Archaeos Tuff has a volume of ~ 89 km^3 and a biostratigraphic age of 520 ka. Druitt et al. (2024) interpreted that this deposit is probably caused by an underwater eruption from an eruption source close to the Early Centres of Akrotiri or the basin between Santorini and Christiana. The Archaeos Tuff has also been found on the islands of Christiani, Santorini and Anafi (e.g. Keller et al., 2010).

Between 550 and 450 ka the Peristeria volcano was active in the northern part of Santorini. During this period also several cinder cones were formed on the Akrotiri Peninsula (e.g. Druitt et al., 1999). From 350 ka to the LBA eruption at least 11 large explosive eruptions occurred (Druitt et al., 2019). Each of the Plinian eruptions consisted of fall deposits and in many cases also surge and flow deposits that were in at least four documented cases followed by a caldera collapse (e.g. Druit et al., 1999). The periods between the Plinian eruptions ("Interplinian") were characterised by effusive and minor explosive volcanism. Each cycle lasted approximately 10–30 ka (Bailey et al., 2009). The last cycle culminated with the LBA eruption (3.6 ka) where 24.5 ± 6.8 km^3 of dense-rock equivalent material has been erupted (Karstens et al., 2023). A new cycle started with the formation of the Kameni Islands, which are at present the most active part of the CSK-VF.

Between Christiana Archipelago and Santorini an eruption centre called Poseidon has been identified by Preine et al. (2022a). Volcanic products from this centre are contemporaneous with the K1–K2 deposits of Kolombo (Preine et al., 2022a) at ~ 1.2 Ma.

2.3 The Christiana Archipelago

The Christiana Archipelago consists of three small islands, Christiani (~ 1.2 km^2), Askania (~ 0.25 km^2) and Eschati (~ 0.01 km^2) that are located approximately 20 km southwest of Santorini (see Fig. 1C). These islands are the remnants of a large conical volcano that rises ~ 500 m from the floor of the Christiana basin (Fig. 1C). This volcanic cone is probably located at the intersection of a pair of fault zones trending NNW–SSE and NNE–SSW (Nomikou et al., 2013). A horseshoe shaped sector-collapse structure of the Christiana volcanic cone can be observed at NE side which produced slump deposit with a volume of ~ 4.9 km^3 (e.g. Preine et al., 2022b). An NNE-SSW fault zone, the Christiana fault, forms the northern wall of this horseshoe shape structure and can be traced further north of Christiani (see Fig. 1B). Preine et al. (2022b) interpreted that this Christiano volcano sector collapse and one on the southeastern flank of proto-Santorini contributed to a large mass transport deposit that occurred ~ 700 ka ago. Three submarine volcanic domes that rise approximately 200–300 m above the seafloor have been observed ca 10 km east of Christiani (Nomikou et al., 2013; Fig. 1C).

A sketch geological map of Christiani island has been published by Mountrakis et al. (1996) which is reproduced in Fig. 2. The stratigraphic sequence consists of the Lower lavas unit, volcaniclastic sequence (pyroclastic material) unit, Upper lavas unit and on top paleosols. Puchelt et al. (1977) described that pyroclastic material is found underneath the lavas (the Upper lavas of Mountrakis et al., 1996) at several locations, whereas both Puchelt et al. (1977) and Aarburg and Frechen (1999) reported that pyroclastic deposits are also found on top of lava flows and in the paleosols. Aarburg and Frechen (1999) distinguished 5 different pyroclastic deposits on top of the Upper lavas and in the paleosols which they called, "Unterer Bims", Lower Pumice (UB); "Oberer Bims", Upper Pumice (OB); "Graue Asche", Grey Ashes (GA); "Schlacken-Fallablagerung", Scoria fall deposit (SF) and "Bims-Fallablagerung", Pumice fall deposits (BF). The Unterer Bims deposit was interpreted by Keller et al. (2010) as derived from a major explosive event in the CSK-VF which they called the Christiani Ignimbrite. Recently, Druitt et al. (2024) further investigated the Christiani Ignimbrite and found that this deposit can be found over a large area surrounding Santorini at water depths of 200–1000 m. They called this deposit the Archaeos Tuff and estimated the total volume to larger than 89 ± 8 km^3 and an eruption age of 520 ± 10 kyr based on biostratigraphy. Pyroclastic deposits derived from Santorini have been reported also from other islands, for example the Lower Pumice 2 pumice deposits on Analfi (Keller et al., 2014).

According to Francalanci et al. (2005), the volcanics of Christiana are chemically similar to the 650–550 ka amphibole bearing andesites-dacites and rhyolites in the SW part of the Akrotiri Peninsula of Santorini. The Christiana Archipelago is composed of andesites, dacites and rhyolites, with rare basaltic andesites. These rocks classify as calc-alkaline, and only dacites plot in the high calc-alkaline field (Francalanci et al., 2005). Most of the rhyolites have high SiO_2 contents (75 wt %–78 wt %).

No isotopic age information is available for the Christiana Archipelago. Correlation of sediments and key seismic reflectors has been used by Piper et al. (2007) and Preine et al. (2021) to determine a relative age for Christiana Archipelago. Piper et al. (2007) proposed that construction of the Christiana volcano probably started around 1.7 Ma ago and that there was an additional period of volcanic activity around 0.6 Ma, contemporaneous with volcanism on the Akrotiri Peninsula of Santorini. On the other hand, Preine et

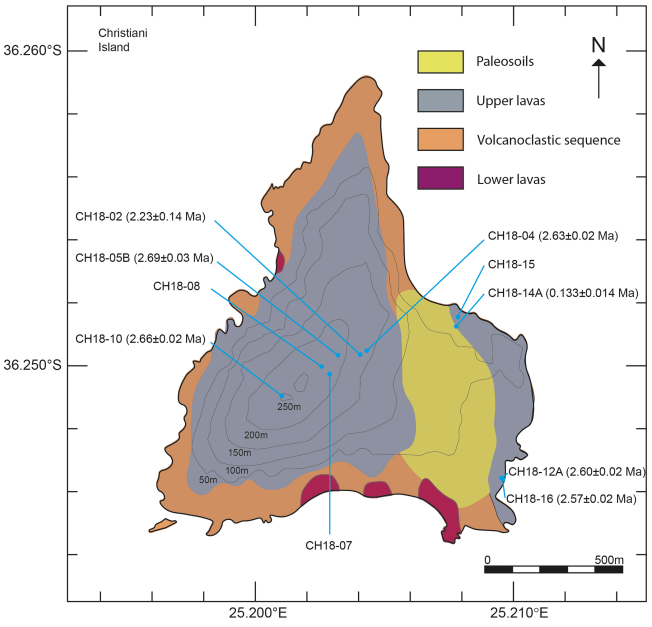

Figure 2. Geological map of Christiani island with sample locations. Map constructed from UGSG Global Multi-resolution Terrain Elevation Data 2010 (GMTED2010) with QGIS contouring. Geological map (after Mountrakis et al., 1996) with sample location. The $^{40}Ar/^{39}Ar$ ages and 2σ errors are from this study and given in brackets, except for samples that did not give a meaningful age (see Table 1).

al. (2021) only observed one period of volcanism (that could have lasted hundreds of thousands of years) around 1.7 Ma. According to Preine et al. (2021), the Christiana volcanic cone is the oldest eruption centre of the CSK-VF.

3 $^{40}Ar/^{39}Ar$ dating methods

3.1 Mineral separation and sample preparation

Twenty-two samples of approximately 1–3 kg were collected from 16 outcrops along the coast and higher parts of Christiani Island (see Fig. 2 and Supplement for sample locations). The samples were cut to approximately 5–10 cm^3 blocks with a diamond saw to remove the weathered surfaces. One of these blocks per sample was used to prepare a thin section to assess the quality and degree of alteration and/or weathering. Twelve of the 22 samples were not suitable for $^{40}Ar/^{39}Ar$ dating because these were affected to a large degree by alteration of the groundmass. The other blocks were cleaned in an ultrasonic bath for 30 min in demi-water, rinsed with demi-water and subsequently dried overnight at 50 °C in a furnace. The selected samples were crushed to chips with a size of < 5 mm in a steel jaw crusher. Approximately 75 % of the crushed sample was further reduced in grainsize in a steel jaw crusher and subsequently sieved to obtain a fraction between 250 and 500 µm for 6 samples and 125–250 µm for 4 samples (see Table 1). Dust was removed from the sieved fractions by ultrasonicating in demi-water for 15 min. Finally, the wet-sieved fractions were dried in a stove at 110 °C.

The groundmass grainsize fraction was separated using multiple steps that included separation by density, magnetic properties and selecting the best grains under a binocular. Groundmass was extracted from the sieved sample fractions by heavy liquid centrifuge density separation techniques (IJlst, 1973). Different densities of heavy liquids were used to obtain groundmass ($2700 \leq \rho \leq 3000\,kg\,m^{-3}$). Magnetic minerals were removed from the groundmass fractions with a Franz Isodynamic Magnet separator. Groundmass grains without visible alteration and inclusions were selected by hand under a binocular optical microscope for the $^{40}Ar/^{39}Ar$ analysis.

3.2 Measurement procedure

The ten groundmass samples were packed in 9 mm diameter aluminium packages and loaded together with the Fish Canyon tuff sanidine standard (Kuiper et al., 2008) in 22 mm diameter and 5 mm high aluminium capsules. The samples and standards were irradiated at the Oregon State University TRIGA reactor for 1.7 h in the CLOCIT position (equivalent to 1 h CLICIT in irradiation batch VU120). After irradiation the samples and standards were unpacked and loaded in 25-hole Cu trays, containing 25 positions of 6 mm for unknowns and 64 positions of 2 mm wide to be used for sanidine standards. The trays were prebaked for 24 h under vacuum at 250 °C and were consecutively placed in the sample chamber and baked at 120 °C. A 50 W Synrad 48-5 Series CO_2 laser was used for fusing the standards and incrementally heating the samples in 10 to 18 steps. The released gas was purified using the Lauda cooler at −70 °C, a NP10 at 400 °C, ST172 at 400 °C and Ti sponge at 500 °C. The cleaned gas was expanded into a ThermoFisher Helix multi-collector mass spectrometer and ^{40}Ar was measured on the H2-Faraday cup connected to an amplifier fitted with a 10^{13} Ohm amplifier in the feed-back loop, ^{39}Ar on the H1-compact discrete dynode (CDD), ^{38}Ar on the AX-CDD, ^{37}Ar on the L1-CDD and ^{36}Ar on the high resolution L2-CDD. Five samples were measured in triplicate, and five samples were measured in duplicate. The heating schedules were optimized in the second and third runs based on data obtained from the first run.

The ArArCalc software (Koppers, 2002) was used for data reduction. The ages were calculated relative to Fish Canyon Tuff sanidine of 28.201 ± 0.023 Ma based on Kuiper et al. (2008). The decay constants of Min et al. (2000) were used. The atmospheric $^{40}Ar/^{36}Ar$ ratio of 298.56 ± 0.31 is based on Lee et al. (2006). The correction factors for neutron interference reactions are $(2.64 \pm 0.02) \times 10^{-4}$ for $(^{36}Ar/^{37}Ar)_{Ca}$, $(6.73 \pm 0.04) \times 10^{-4}$ for $(^{39}Ar/^{37}Ar)_{Ca}$, $(1.21 \pm 0.003) \times 10^{-2}$ for $(^{38}Ar/^{39}Ar)_{K}$ and $(8.6 \pm 0.7) \times 10^{-4}$ for $(^{40}Ar/^{39}Ar)_{K}$. The gain corrections for all ampli-

Table 1. Summary of $^{40}Ar/^{39}Ar$ data. Ages in bold are accepted as meaningful ages, in italic are rejected (see text for discussion). NA = not available.

	Age (Ma)	±2σ (Ma)	MSWD	*N*	N_{total}	$^{39}Ar_K$ (%)	K/Ca	±2σ	$^{40}Ar/^{36}Ar$	±2σ	Age (Ma)	±2σ (Ma)	MSWD
CH18-02 – Christiana – groundmass – 400–500 μm													
VU120-O1a	2.53	0.32	0.28	2	12	48.1	0.65	0.14	NA	NA	NA	NA	NA
VU120-O1b	2.17	0.21	1.65	8	13	72.3	0.42	0.13	295.5	2.9	2.72	0.52	1.16
VU120-O1c	2.27	0.20	2.30	5	12	54.6	0.38	0.14	301.8	3.6	1.72	0.61	1.73
VU120-O1b, c	**2.23**	**0.14**	1.81	13	25	63.4	0.40	0.09	298.6	2.8	2.23	0.48	2.21
CH18-07 – Christiana – groundmass – 400–500 μm													
VU120-O2a	2.69	0.05	5.81	5	12	66.4	0.26	0.13	285.1	27.1	2.88	0.38	6.21
VU120-O2b	2.67	0.03	1.56	9	12	82.4	0.25	0.11	287.8	6.8	2.82	0.10	0.46
VU120-O2c	2.69	0.04	2.69	8	12	75.4	0.27	0.09	294.0	19.9	2.75	0.29	3.15
VU120-O2a, b, c	*2.68*	*0.03*	2.46	22	36	74.4	0.26	0.06	289.1	7.3	2.82	0.11	2.03
CH18-12A – Christiana – groundmass – 400–500 μm													
VU120-O3a	2.61	0.03	1.75	8	12	94.0	0.19	0.07	299.5	4.6	2.60	0.07	2.04
VU120-O3b	2.57	0.07	2.56	9	13	80.6	0.28	0.05	292.1	7.6	2.66	0.12	2.10
VU120-O3c	2.60	0.02	0.93	8	13	67.6	0.27	0.06	302.6	5.4	2.59	0.03	0.71
VU120-O3a, b, c	**2.60**	**0.02**	1.52	24	38	76.9	0.23	0.04	297.8	2.4	2.60	0.03	1.57
CH18-15 – Christiana – groundmass – 400–500 μm													
VU120-O5a	2.48	0.13	0.87	7	10	98.74	0.25	0.17	300.2	2.2	2.22	0.37	0.71
VU120-O5b	2.19	0.13	1.31	17	18	99.25	0.15	0.07	299.8	1.5	1.98	0.28	1.26
VU120-O5c	2.50	0.10	1.82	14	18	92.17	0.34	0.12	298.4	1.7	2.53	0.28	2.24
VU120-O5a, b, c	*2.42*	*0.08*	1.90	37	46	95.73	0.18	0.05	298.7	1.2	2.40	0.20	2.12
CH18-16 – Christiana – groundmass – 400–500 μm													
VU120-O6a	2.61	0.03	0.76	5	11	74.75	0.43	0.16	299.7	5.2	2.59	0.11	1.00
VU120-O6b	2.54	0.03	1.82	10	17	66.99	0.37	0.12	293.6	3.6	2.62	0.06	1.09
VU120-O6a, b	**2.57**	**0.02**	1.80	13	28	64.90	0.49	0.10	302.2	4.7	2.51	0.08	1.68
CH18-04 – Christiana – groundmass – 125-250μm													
VU120-O7a	2.63	0.02	1.66	9	12	98.32	0.42	0.08	298.0	3.5	2.64	0.03	1.88
VU120-O7b	2.63	0.02	1.29	7	11	81.68	0.48	0.10	282.2	12.3	2.66	0.04	0.23
VU120-O7a, b	**2.63**	**0.02**	1.42	16	23	89.82	0.44	0.06	297.7	2.9	2.63	0.02	1.49
CH19-05B – Christiana – groundmass – 125-250μm													
VU120-O8a	2.66	0.05	1.34	8	12	85.80	0.37	0.03	285.1	13.3	2.76	0.10	0.94
VU120-O8b	2.70	0.04	1.38	8	10	89.86	0.39	0.04	286.9	16.4	2.77	0.11	1.22
VU120-O8a, b	**2.69**	**0.03**	1.45	16	22	87.97	0.38	0.02	284.8	9.7	2.78	0.07	1.01
CH18-08 – Christiana – groundmass – 125-250μm													
VU120-O9a	2.75	0.04	0.90	8	12	94.03	0.24	0.09	297.0	4.2	2.79	0.11	1.00
VU120-O9b	2.74	0.06	4.59	5	10	59.36	0.20	0.10	295.9	9.6	2.79	0.17	5.70
VU120-O9a, b	*2.75*	*0.04*	2.06	13	22	72.70	0.22	0.06	297.0	3.8	2.78	0.08	2.17
CH18-10 – Christiana – groundmass – 125-250μm													
VU120-O10a	2.66	0.02	4.03	5	12	76.66	0.44	0.04	288.5	13.7	2.69	0.05	3.24
VU120-O10b	2.65	0.03	0.60	8	12	71.90	0.46	0.02	287.7	13.6	2.69	0.05	0.29
VU120-O10a, b	**2.66**	**0.02**	1.69	13	24	74.43	0.45	0.02	288.4	6.8	2.69	0.03	1.05
	Age (ka)	±2σ (ka)	MSWD	*N*	N_{total}	$^{39}Ar_K$ (%)	K/Ca	±2σ	$^{40}Ar/^{36}Ar$	±2σ	Age (ka)	±2σ (ka)	MSWD
CH18-14A – Christiana – obsidian groundmass – 400–500 μm													
VU120-O4a	222	91	2.57	9	12	99.7	0.51	0.04	301.9	1.8	94.6	56.2	1.04
VU120-O4b	139	19	0.61	9	10	99.9	0.50	0.05	296.6	4.7	148.4	28.4	0.60
VU120-O4c	124	18	0.88	9	10	99.8	0.50	0.06	304.8	5.4	108.6	22.5	0.22
VU120-O4a, b, c	**133**	**14**	1.10	25	32	87.3	0.50	0.03	301.0	1.7	**122.6**	**14.6**	0.79

fiers (calculated relative to the AX-CDD) were determined by peak jumping of a ~ 5.5 fA beam of CO_2 in dynamic mode. The gain corrections factors and their standard errors during this study were: 0.96718 ± 0.00029 for H2-Far, 0.98652 ± 0.00012 for H1-CDD, 1.00465 ± 0.0011 for L2-CDD, and 0.96637 ± 0.00027 for L2-CDD. The errors listed above are quoted at the 1σ level. Results below are reported at the 2σ level and include all analytical errors. All relevant analytical data for the age calculations can be found in the Supplement.

4 Results

Petrographic descriptions can be found in the Supplement and are summarised in Fig. 3. All collected samples are porphyritic (except CH18-14A), and the most common phenocrysts are plagioclase, clinopyroxene and orthopyroxene (see Fig. 3). Two samples (CH18-02 and CH18-15) contain amphibole. Sample CH18-14A is an obsidian collected from the east coast. This sample contains brownish altered glass and small crystals of quartz, plagioclase and orthopyroxene.

Table 1 reports the $^{40}Ar/^{39}Ar$ ages that were obtained for 10 volcanic samples of Christiani. The detailed datasets and diagrams of the age spectra, inverse isochrons and Ca/K spectra can be found in Figs. 4, 5, and Supplement. Ages are based on plateaus in the age spectra and defined as three or more consecutive steps representing $> 50\,\%$ of the total released $^{39}Ar_K$ and p values > 0.05. All errors are reported as 2σ. The results can be divided into two groups. Sample VU120-O4 (CH18-14A) has an age of ~ 133 ka, while the rest of the samples range from 2.23 to 2.82 Ma, with the majority between 2.6–2.7 Ma. The analytical uncertainties are low (0.02–0.14 Ma) and the spectra of the individual samples are discussed below.

The spectra of experiment VU120-O1 (sample CH18-02) (Fig. 4) shows a relatively large uncertainty (0.14 Ma), due to the large atmospheric correction as result of relatively high ^{36}Ar intensities for experiment VU120-O1a. The experiments VU120-O1a and b show similar plateaus at 2.17 ± 0.21 Ma for run b (MSWD $= 1.65$, $n = 8$, $n_{total} = 13$) representing 72.3 % of ^{39}Ar released ($^{39}Ar_K$ (%)), and 2.27 ± 0.20 Ma for run c (MSWD $= 2.30$, $n = 5$, $n_{total} = 12$, $^{39}Ar_K$ (%) $= 54.6$). This yields a weighted mean age of 2.23 ± 0.14 Ma (MSWD $= 1.81$). The obtained ages are relatively constant with increasing temperature. The inverse isochron age is 2.23 ± 0.48 Ma (MSWD $= 2.22$, Fig. 5), which is indistinguishable from the plateau age, due to the $^{40}Ar/^{36}Ar$ ratio being equal to atmosphere (298.56). The relatively high uncertainty is caused by the low radiogenic ^{40}Ar yield of ~ 3.51 % for run b and ~ 4.06 % for run c. This suggests that this sample might have been altered and has lost some radiogenic argon during this process, resulting in a too young age. However, petrography of this sample (see Supplement) shows only minor alteration of olivine and matrix and has a relatively low LOI of 0.58 wt %.

Figure 4 shows the age spectra of experiment VU120-O2 (sample CH18-07) and is characterised by stable plateau's and overlapping spectra. Experiment VU120-O2a yields an age of 2.69 ± 0.05 Ma (MSWD $= 5.814$, $N = 5$, $n_{total} = 12$, $^{39}Ar_K$ (%) $= 66.4$), experiment b yields 2.67 ± 0.03 Ma (MSWD $= 1.56$, $N = 9$, $n_{total} = 12$, $^{39}Ar_K$ (%) $= 82.4$) and run c yields 2.69 ± 0.04 Ma (MSWD $= 2.69$, $N = 8$, $n_{total} = 12$, $^{39}Ar_K$ (%) $= 75.4$). The high MSDW value and $p = 0.0005$ suggest that this is not a reliable age and we will not discuss this sample further.

Results of experiment VU120-O3 (sample CH18-12A) are shown in Fig. 4. The three experiments yield the following ages: a $= 2.61 \pm 0.03$ Ma (MSWD $= 1.75$, $N = 8$, $n_{total} = 12$, $^{39}Ar_K$ (%) $= 94$), b $= 2.57 \pm 0.07$ Ma (MSWD $= 2.56$, $N = 9$, $n_{total} = 13$, $^{39}Ar_K$ (%) $= 80.6$) and c $= 2.60 \pm 0.02$ Ma (MSWD $= 0.93$, $N = 8$, $n_{total} = 13$, $^{39}Ar_K$ (%) $= 67.6$). This results in a weighted mean age of 2.60 ± 0.02 Ma (MSWD $= 1.52$). The inverse isochron age is 2.60 ± 0.03 Ma (Fig. 5) which is indistinguishable from the weighted mean age.

Experiment VU120-O4 (sample CH18-14A) is shown in Fig. 4. The three experiments yield: a $= 222 \pm 91$ ka (MSWD $= 2.57$, $N = 9$, $n_{total} = 12$, $^{39}Ar_K$ (%) $= 99.7$), b $= 139 \pm 19$ ka (MSWD $= 0.61$, $N = 9$, $n_{total} = 10$, $^{39}Ar_K$ (%) $= 99.9$), c $= 124 \pm 18$ ka (MSWD $= 99.8$, $N = 9$, $n_{total} = 10$, $^{39}Ar_K$ (%) $= 99.8$). The weighted mean age is 133 ± 14 ka (MSWD $= 1.1$) and an inverted isochron age of 122.6 ± 14.6 ka (Fig. 5). This is the reported age because of a slight excess of $^{40}Ar^*$, the $^{40}Ar/^{36}Ar$ intercepts at 301.0 ± 1.8 as shown in Fig. 5. The radiogenic ^{40}Ar content is ~ 9 % which is normal for this age interval.

Figure 4 shows the age spectra of 3 runs of experiment VU120-O5 (CH18-15) that yield: a $= 2.48 \pm 0.13$ Ma (MSWD $= 0.87$, $N = 7$, $n_{total} = 10$, $^{39}Ar_K$ (%) $= 98.74$), b $= 2.19 \pm 0.13$ Ma (MSWD $= 1.31$, $N = 17$, $n_{total} = 18$, $^{39}Ar_K$ (%) $= 99.25$) and c $= 2.50 \pm 0.10$ Ma (MSWD $= 1.82$, $N = 14$, $n_{total} = 18$, $^{39}Ar_K$ (%) $= 92.17$). The weighted mean age is 2.42 ± 0.08 Ma (MSWD $= 1.90$) and the inverse isochron age is 2.40 ± 0.20 Ma (MSWD $= 2.12$, Fig. 5), which is identical to the mean age. However, the measurements were characterized by low radiogenic ^{40}Ar yields (a $= \sim 4.14$ %, b $= \sim 3.44$ % and c $= \sim 4.69$ %), which could result in a reported age that is too young. In addition, the p value for this sample is very low (0.0015), suggesting that this is not a meaningful age. We will therefore not discuss it further.

Experiment VU120-O6 (sample CH18-16, Fig. 4): run a yields 2.61 ± 0.03 Ma (MSWD $= 0.76$, $N = 9$, $n_{total} = 11$, $^{39}Ar_K$ (%) $= 74.75$) and run b yields 2.54 ± 0.03 Ma (MSWD $= 1.82$, $N = 10$, $n_{total} = 17$, $^{39}Ar_K$ (%) $= 66.99$) resulting in a weighted mean age of 2.57 ± 0.02 Ma (MSWD $= 1.8$). The inverse isochron age is 2.51 ± 0.08 Ma, which is within error of the age plateau (Fig. 5).

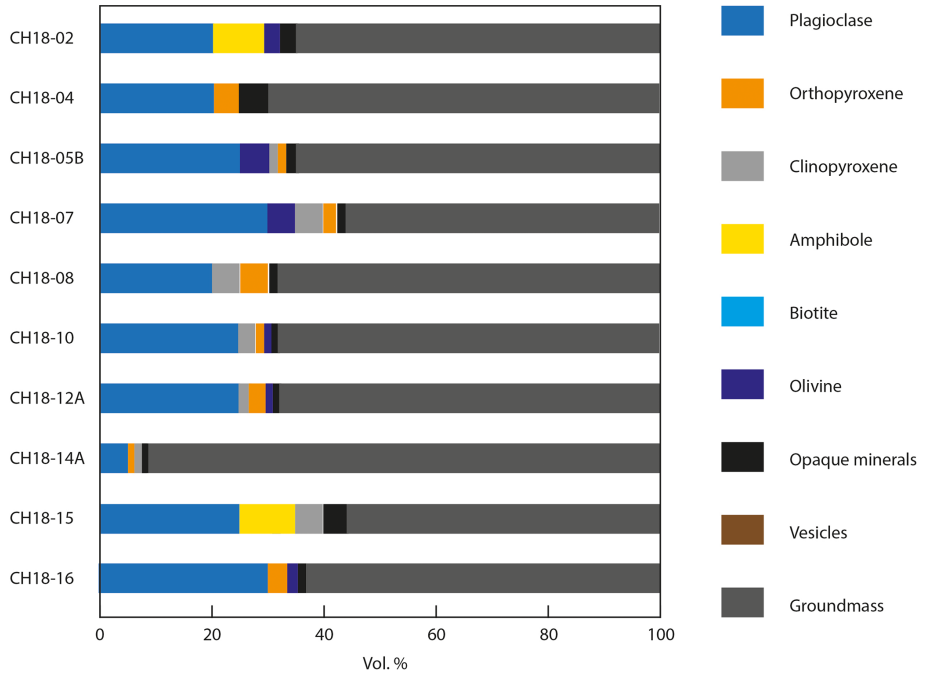

Figure 3. Modal composition (phenocrysts/groundmass/vesicles) of the studied samples from Christiani island.

Figure 3 shows the age spectra of experiment VU120-O7 (sample CH18-04) where run a yields 2.63 ± 0.02 Ma (MSWD $= 1.66$, $N = 9$, $n_{total} = 12$, $^{39}Ar_K$ (%) $= 98.32$) and run b yields 2.63 ± 0.02 Ma (MSWD $= 1.29$, $N = 7$, $n_{total} = 11$, $^{39}Ar_K$ (%) $= 81.68$) giving a weighted mean age of: 2.63 ± 0.02 Ma (MSWD $= 1.42$). The inverse isochron age is 2.66 ± 0.04 Ma (MSWD $= 0.23$) which is within error of the age plateau age (Fig. 5).

Age plateaus of experiment VU120-O8 (sample CH18-05B) are shown in Fig. 4. Run a yields: 2.66 ± 0.05 Ma (MSWD $= 1.34$, $N = 8$, $n_{total} = 12$, $^{39}Ar_K$ (%) $= 85.8$) and run b yields: 2.70 ± 0.04 Ma (MSWD $= 1.38$, $N = 8$, $n_{total} = 10$, $^{39}Ar_K$ (%) $= 89.86$) giving a weighted mean age of 2.69 ± 0.03 Ma (MSWD $= 1.45$). The inverse isochron age is 2.76 ± 0.10 Ma (MSWD $= 0.94$) which is within error of the weighted mean plateau age (Fig. 4).

Figure 4 shows the age plateaus of experiment VU120-O9 (sample CH18-08) where run a and b yields: 2.75 ± 0.04 Ma (MSWD $= 0.90$, $N = 8$, $n_{total} = 12$, $^{39}Ar_K$ (%) $= 94.03$) and 2.74 ± 0.06 Ma (MSWD $= 4.59$, $N = 5$, $n_{total} = 10$, $^{39}Ar_K$ (%) $= 59.36$), respectively. The low p value for the average of this sample (0.03) indicates that this is not a reliable age and we will not further discuss it.

Experiment VU120-O10 (sample CH18-10) (Fig. 4) was analysed in duplicate. Run a and b yields: 2.65 ± 0.03 Ma (MSWD $= 0.60$, $N = 8$, $n_{total} = 12$, $^{39}Ar_K$ (%) $= 71.90$) and 2.66 ± 0.02 Ma (MSWD $= 4.03$, $N = 5$, $n_{total} = 12$, $^{39}Ar_K$ (%) $= 76.66$), respectively. The weighted mean age of run a and b is 2.66 ± 0.02 Ma (MSWD $= 1.69$). The inverse isochron age is 2.69 ± 0.05 Ma (MSWD $= 3.24$, Fig. 5) which is within error of the weighted mean age.

The geographical distribution of the $^{40}Ar/^{39}Ar$ ages is shown in Fig. 2. The $^{40}Ar/^{39}Ar$ ages cluster around 2.63 ± 0.05 Ma (1 sd, $n = 5$) (excluding sample CH18-02). Sample CH18-14B gave a much younger $^{40}Ar/^{39}Ar$ age of 133 ± 14 kyr.

5 Discussion

5.1 Data quality

Based on the MDSW and p values of the $^{40}Ar/^{39}Ar$ results, experiment VU120-O2 (sample CH18-07); VU120-O5 (CH18-15) and VU120-O9 (CH18-08) are rejected as meaningful ages following the protocol of Schaen et al. (2021). The uncertainty of the obtained ages is small, in general less than 1 % apart from experiments VU120-O1 (6.1 %) and VU120-O4 (10.1 %). Experiment VU120-O1 produced low yields of radiogenic ^{40}Ar and thus contained a large component of non-radiogenic argon (see Fig. 6A). This could influence the precision and accuracy of the obtained age and result in an age that is more susceptible to bias, either too young in case of minor alteration, or too old in the case of inheritance of a small component of magma chamber based ambient, excess argon. Figure 6B shows that samples with a larger age error (> 0.08 Ma) are indeed younger than the samples with smaller error bars (< 0.04 Ma).

Another possibility is that sample CH18-02 did not behave as a closed system and that Ar and/or K have been re-

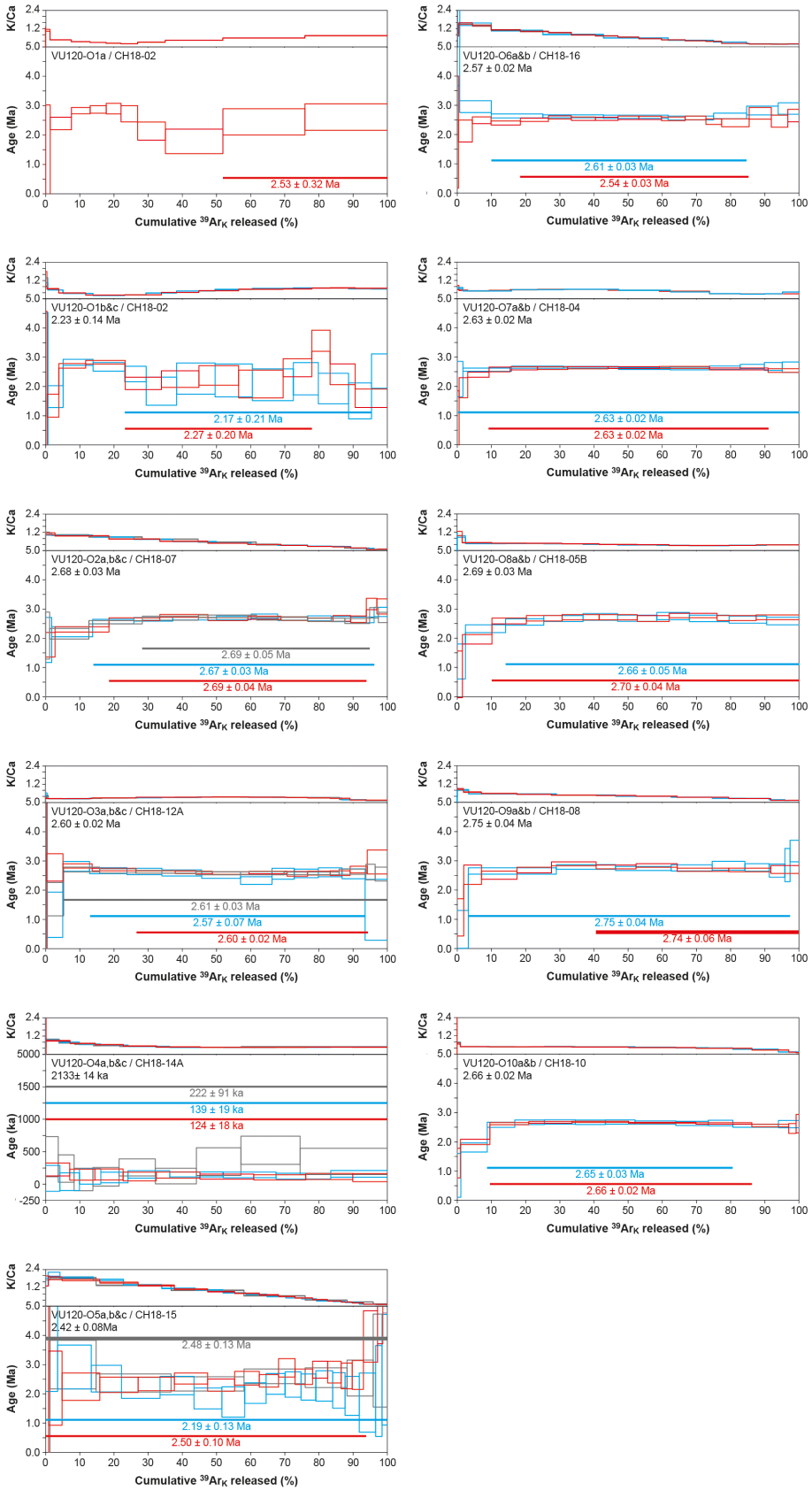

Figure 4. Cumulative $^{39}Ar_K$ released versus age and K/Ca ratio for Christiani samples. See text for discussion.

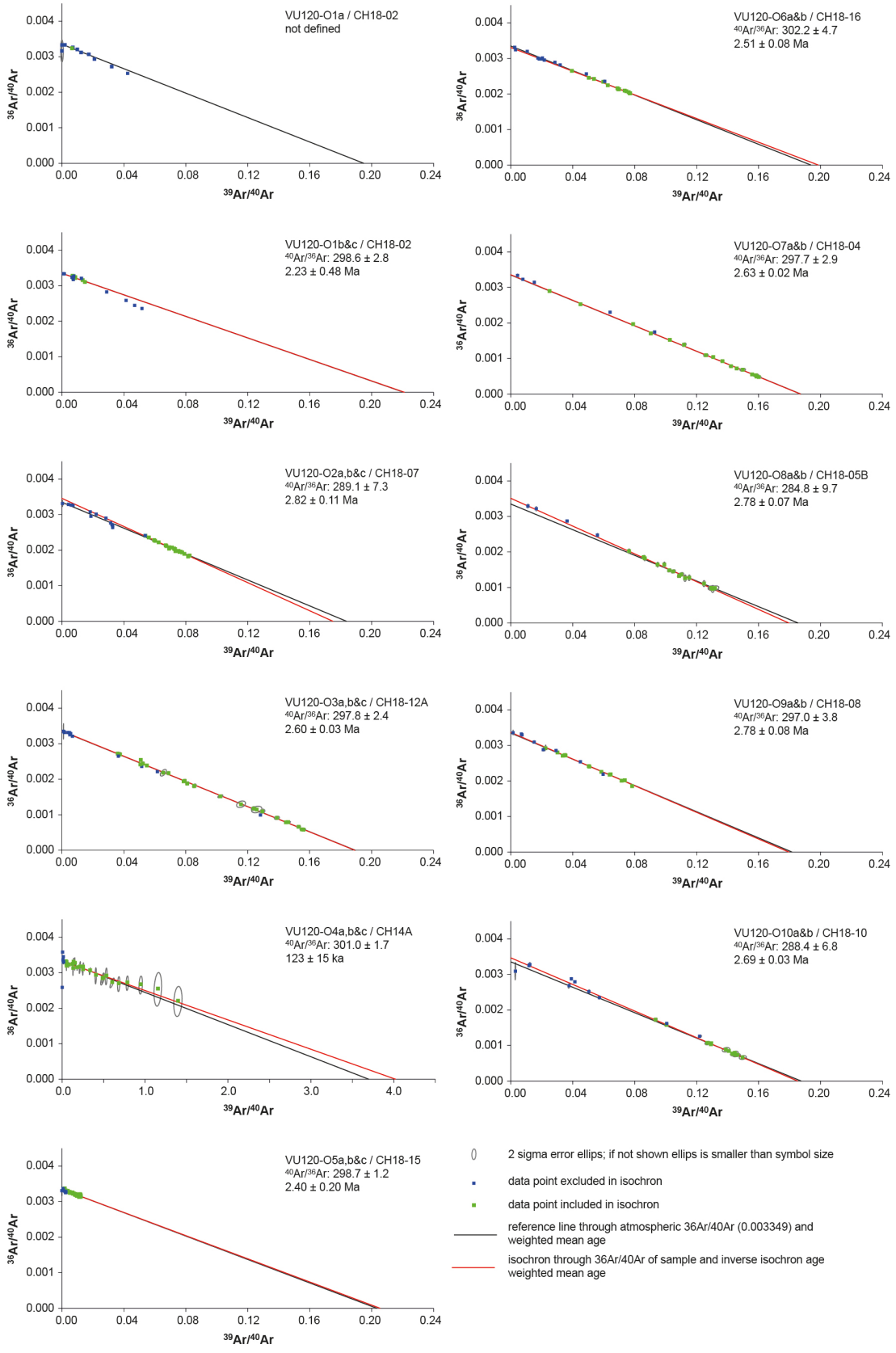

Figure 5. $^{39}Ar/^{40}Ar$ versus $^{36}Ar/^{40}Ar$ isochrons. See text for discussion.

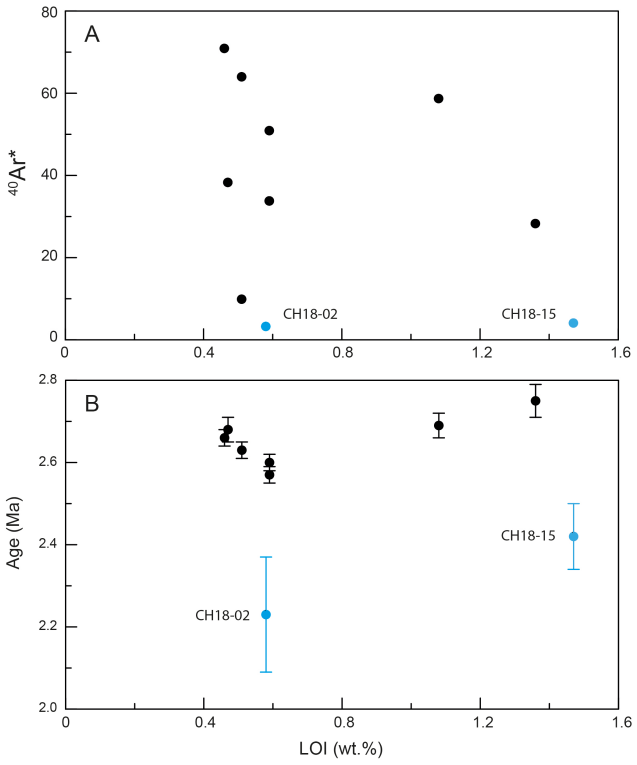

Figure 6. LOI versus **(A)** $^{40}Ar^*$ and **(B)** Age. Three samples that did not provide a meaningful age are also included (see Table 1). Black symbols are samples without amphibole, samples CH18-02 and CH18-15 (blue symbols) do contain amphibole. Sample CH18-14A is omitted from **(B)** due to its very young age of 0.133 Ma. Error bars are 2σ. See text for discussion.

moved or added, for example during alteration of minerals and/or groundmass (e.g. Castellanos Melendez et al., 2023). The loss of ignition (LOI) can be used as an indicator for the degree alteration of a sample, the more groundmass/minerals are converted to clay minerals the higher the LOI will be. Figure 6 shows the LOI versus $^{40}Ar^*$ and age. The lowest $^{40}Ar^*$ and largest age errors are observed in the two samples that contain amphibole. There are no correlations between LOI and $^{40}Ar^*$ and age, suggesting that alteration did probably not affect the ages of these samples. It should be noted that all samples were selected for minimal alteration (by optical microscope, see methods).

Experiment VU120-O4 (Sample CH18-14A) is the only sample with an age of 133 ka, all other samples range between 2.2 and 2.8 Ma. The relative uncertainty of VU120-O4 is higher, even while the absolute uncertainty is only 14 kyr, compared to 20–80 kyr for the other samples. The young $^{40}Ar/^{39}Ar$ age of VU120-O4/CH18-14A will be discussed below.

Three experiments (VU120-O2, O8 and O10) show a subatmospheric $^{40}Ar/^{36}Ar$ ratio (289, 285 and 288, respectively, see Fig. 5). This has been attributed to $^{40}Ar^*$ loss (Heath et al., 2018, and references therein) and result in an older inverse isochron age (Fig. 5) then the plateau age. Despite the deviations between the isochron age and the plateau ages, we believe that the plateau ages are the best estimate for the accurate eruption age for experiments VU120-O2 and O8. Experiment VU120-O10 plateau and isochron ages are within error of each other.

5.2 How representative are these ages for the age of Christiana volcano?

The average age of the studied samples is 2.64 ± 0.05 Ma (2 sd, $n = 5$) if we exclude samples with a large error (CH18-02) and anomalous young age (CH18-14A). The samples collected for this study are only representative for a small volume of the Christiana volcano and all (except CH18-14A) derived from the Upper lavas (Fig. 2; Mountrakis et al., 1996). The submarine part of this volcano (> 80 %) and volcanic deposits of the two other islands (Askania and Eschati, see Fig. 1C) have not been studied. Furthermore, 6 of the 10 samples were collected from the main fault plane (Samples CH18-02, 04, 05B, 06, 08 and 10, see Figs. 1C and 2) whereas CH18-12A, 14A, 15 and 16 were collected from the cliffs on the eastern side of the island (see Fig. 2). Although these samples are from another part of the island, the ages are comparable to those obtained from samples from the fault plane (Fig. 2; Mountrakis et al., 1996). This suggests that the present-day top of the Christiani was constructed of large volumes of lavas around 2.6 Ma, and that the submarine part could be older than 2.6 Ma. A rough estimate of the present-day volume of the cone of the Christiana volcano based on the bathymetry map of Fig. 1C gives a minimum volume of $\sim 25\,km^3$. This estimate ignores erosion, submarine mass slumps and pyroclastic material dispersed further away from the volcanic cone. If the Christiana volcano was constructed with the same magma production rate as Santorini ($1\,km^3\,kyr^{-1}$, Druitt et al., 1999), the whole cone would have been constructed in minimal ~ 25 kyr. Samples from the submarine part of Christiana volcano and the domes east of the Cristiana Archipelago (Fig. 1C) are required to verify if the complete cone of Christiana volcano was constructed in such a short timeframe.

Sample VU120-O4 (CH18-14B), with an age of 113 ka, is significantly younger than the other samples. This sample shows a slight excess argon signal; however, it should be noted that the radiogenic ^{40}Ar content is ~ 9 %, which is commonly observed for obsidians in this age interval (e.g. Branca et al., 2008). While the total data set shows a tight age range, the obsidian sample is significantly younger than all the other samples. This sample is the only obsidian sample and is a lithic fragment from a pyroclastic flow. There are two possible scenarios for the presence of this young age: (1) it is

derived from a young eruption of the Christiana archipelago, perhaps a submarine eruption; (2) it is derived from Santorini as a lithic block in pyroclastic deposit.

It is not very likely that this obsidian sample is derived from Christiana volcano itself, since the volcano probably was extinct for the last 1.5 Ma (e.g. Preine et al., 2021). The obsidian clast can also be derived from Santorini, as remnants of a large ignimbrite deposit were reported by Keller et al. (2010) on the islands of Santorini, Christiani and Anafi. On Christiani these deposits were first described by Puchelt et al. (1977) as the "Christiani pumice" and later as "Unterer Bims" by Aarburg and Frechen (1999). Druitt et al. (2024) linked the subarial and marine pumice deposits to one large eruption and called the deposit the Archaeos Tuff. The eruption that is responsible for this tuff took place 520 ka year ago and was probably derived from a submarine vent in the neighbourhood of the Akrotiri peninsula of Santorini. As described above, Aarburg and Frechen (1999) described 4 more pyroclastic units above the Unterer Bims (or Archaeos Tuff) that are not derived from Christiani. The Milos VF is approximately 100 km away from Christiani and probably too far away for pyroclastic flows to reach Christiana volcano. On the other hand, Santorini/Kolombo are approximately 25–40 km away and it is therefore far more likely that fall and flow deposits are derived from these volcanoes. Sample CH18-14 is younger than the Archaeos Tuff eruption, but it could be related to one of the Plinian eruptions in the interval 160–80 ka. In this interval there are three dated Plinian pyroclastic deposits, Cape Thera $\sim$ 160 ka, Middle Pumice $\sim$ 145 ka, Upper Scoria $\sim$ 81 ka (e.g. Druitt et al., 1999). The Vourvoulos deposit has not been dated yet but should have an age between the Middle Pumice and Upper Scoria, e.g. $\sim$ 145–81 ka. The age for CH18-14 is 133 ± 14 ka and taking the error into account, the age overlaps with that of the Middle Pumice. Since this is a lithic fragment, we assume that the high temperature of a pyroclastic flow did completely reset the K-Ar system. If the K-Ar system was not (or not completely) reset by the exposure to high temperatures of the eruption, it must have been transported by a pyroclastic flow or fall deposit with an age younger than 133 ka.

5.3 Geochronological evolution of the Christiana volcano

The $^{40}Ar/^{39}Ar$ ages of volcanic rocks from Christiani obtained during this study differs significantly from what was proposed as the age of the Christiana volcano either by correlation (Piper et al., 2007), or sub-marine seismic interpretation (Preine et al., 2021), although we confirm their notion that the Christiana volcano is significantly older than the Santorini and Kolumbo volcanoes. Francalanci et al. (2005) argued on geochemical grounds that the Christiana volcanics are contemporaneous with the dacites of Akrotiri, that are dated at 650–550 ka (Druitt et al., 1999), some 2 Myr younger than the ages we obtained in this study for subaerial Upper lava Christiana samples (Mountrakis et al., 1996). Piper et al. (2007) have correlated the emergence of Christiana volcano to a reflector in the subsurface that is dated at approximately 2 Ma. Piper et al.'s (2007) study describes a two-stage evolution for Christiana, a minor older stage with volcanic activity of Pliocene age ($>$ 2.5 Ma) and a younger stage with volcanic activity that occurs in the same interval as the dacitic lava flows and cinder cones of Akrotiri, i.e. 650–450 ka. The ages used by Piper et al. (2007) are estimates based on seismic reflector studies and correlation with dated sediments. The $^{40}Ar/^{39}Ar$ age data from this study shows that the Upper Lavas range between 2.69–2.57 Ma (see above) which correlates to the minor older stage volcanic activity of Piper et al. (2007). The younger stage (650–450 ka) that was proposed by Piper et al. (2007) is not observed in our data set (see Fig. 2).

5.4 Comparison with other SAVA volcanic fields

The Christiani $^{40}Ar/^{39}Ar$ ages of this study are compared to other age data of the VF of the SAVA and older magmatic products from the Aegean Sea and western Anatolia (Fig. 7A). Volcanism of Christiani overlaps in age with the youngest eruptions of the Sousaki VF (East), Methana, Poros and the youngest products of Aegina of the APM VF (see Fig. 1A). Volcanics of Christiana also overlap with Milos phase 1 and volcanics of Polyegos of the Milos-VF and the Kefalos dacite deposit of the Kos-Nisyros-Yali VF. This suggests that all 5 VFs of the SAVA were active in the period 3.0–2.5 Ma. Volcanism in the western sector probably started around 4–5 Ma years ago in the western Sousaki and Aegina-Poros-Methana VF (Vougioukalakis et al., 2019) whereas for the central (Milos and CSK VF) and eastern sector (KNY-VF) the oldest dated deposits are $\sim$ 3.0 Ma old (This study; Bachmann et al., 2010; Zhou et al., 2021; Vougioukalakis et al., 2019).

Many studies of the SAVA have stressed that the volcanic output of the volcanic centres is controlled by the local tectonic stress field in the upper crust (e.g. Nomikou et al., 2013; Pe-Piper and Piper, 2013; Elburg et al., 2018; Preine et al., 2022b). Figure 7B shows the changes in the tectonic stress field orientation over time in the northern, central and eastern part of the SAVA from 0–5 Ma. In all VF there was a gradual change in the tectonic stress field during the past 3 Ma that resulted in different fault systems to be activated (see Fig. 7B). During the Pliocene the NW-SE Christiana Graben formed due to NNE-SSW extension. (Fig. 7B; Heath et al., 2019; Preine et al., 2022a). The Christiana volcano was active when the CSK rift was characterised by NNE-SSW extension (see Fig. 7B). In the interval of $\sim$ 2.5–1.5 Ma the stress field rotated from NNE-SSW to NW-SE (see Fig. 7B) and the CSK rift developed with volcanic deposits of Poseidon and Kolumbo (K1 + K2). Heath et al. (2019) argued that Christiana volcano probably developed because it is located at a junction of NNW-SSE and NE-SW oriented faults. How-

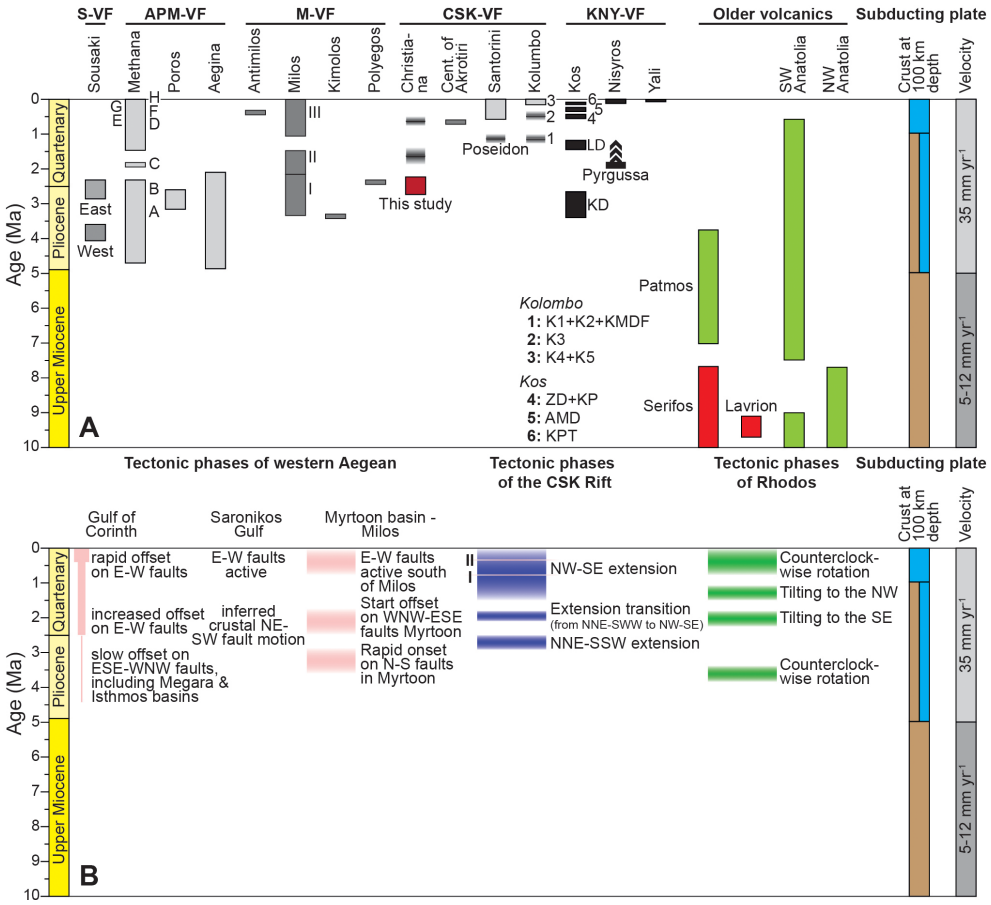

Figure 7. **(A)** Age distribution for the different volcanic fields of the South Aegean Volcanic Arc and older volcanics from Western Anatolia and the Aegean Sea. Abbreviations S-VF, Sousaki volcanic field; APM-VF, Aegina-Poros-Methana volcanic field, M-VF, Milos volcanic field, CSK-VF, Christiana-Santorini-Kolombo volcanic field, KNY-VF, Kos-Nisyros-Yali volcanic field. The east-west Sousaki volcanic field data are from Vougioukalakis et al. (2019) and references therein. The different phases for Methana are labelled A–H (Pe-Piper and Piper, 2013). The volcanic periods of Milos are labelled I, II and III (Zhou et al., 2021). The shaded fields are ages derived from seismic profiles and sedimentation rates for Christiana volcanics and the Poseidon centre (Preine et al., 2021). The new ages for subareal Christiana volcanics from this study are indicated with a red box. Label KMFD, K1–K5 are volcanic phases of Kolombo (Hubscher et al., 2015). The volcanic deposits of Kos are: KPT = Kos Plateau Tuf (Smith et al., 1996) AMD = Agios Mammas dome, ZD = Zini dome, KP = Kefalos series pyroclastics, KD = Kefalos dacite (Bachmann et al., 2010, and ages reported therein). The age for Pyrgussa is from Piper et al. (2019). Arrows indicate that due to excess ^{40}Ar this is the maximum age. Nisyros ages are from Popa et al. (2020). The ages from Patmos are from Boehm et al. (2023). Data for Serifos, Lavrion, NW and SW Anatolia are from Schaarschmidt et al. (2021) and Altunkaynak et al. (2012) and sources in these publications. Nature of the subducted crust and the subduction velocity are after Schaarschmidt et al. (2021). **(B)** Tectonic events in Aegean Sea, based on compilations by Pe-Piper and Piper (2013) for the western Aegean and on Preine et al. (2022a) for the CSK rift and Rhodos region.

ever, our new age data suggest that Christiano volcano was already active when the stress field was predominately NNE-SSW and was probably not active anymore when the stress field changed to NW-SE.

In the CSK-VF there is a long period of quiescence or low volcanic output between 2.4 and 1.2 Ma (see Fig. 7A). During this time interval there are also periods of quiescence or low volcanic output in the S-VF, AFM-VF, M-VF and KNY-VF. The Sousaki VF last intrusions are around 2.3 Ma. In the APM-VF volcanic activity of Poros and Aegina stops at 2.5 and 2.1 Ma, respectively, whereas Methana has two periods of quiescence between 2.4 and 1.5 Ma. On the other hand, the M-VF shows a period of high volcanic output (Period II, Zhou et al., 2021) with a long period without volcanic eruptions between 1.5 and 1.1 Ma. The KNY-VF is probably also characterised by a significant period of quiescence or low volcanic output between 3.0 and 1.0 Ma. Although the timing and volumes of volcanic deposits are different for each VF, they all are characterised by periods of low volcanic output and/or quiescence between 2.0–1.0 Ma. During this time interval the stress field (but with different orientations) changed in all VF, suggesting that parental magmas

have more difficulty to reach the surface during this interval. Hence, the alternation between volcanic eruptions and quiescence is controlled by the local stress field, and not by major tectonic changes on a larger scale (e.g. continental versus oceanic crust subduction).

5.5 Comparison with Upper Miocene-Pliocene Aegean/Western Anatolian volcanics and intrusions

The Aegean Sea and Western Anatolia regions have been characterised by an extended period of pulsed magmatism for over 30 Ma years (e.g. Schaarschmidt et al., 2021). The volcanic and intrusive products have a wide range in compositions with calc-alkaline characteristics with large variations in potassium content and some sodium rich products (e.g. Patmos, Boehm et al., 2023). The volcanic and magmatic products do display younger ages towards the southwest (e.g. Schaarschmidt et al., 2021), ranging from 32 Ma in the NE (Rhodope) to 0 at the present SAVA.

The Aegean microplate was constructed from the accretion of continental and oceanic fragments during the subduction of one continuous slab (Wortel and Spakman, 2000) or three different remnants of slabs (Wei et al., 2019). The nature of the subducted crust at 100 km depth beneath the Aegean plate has changed after the closure of the Pindos Ocean ($\sim$ 35 Ma) to subducted continental crust of the Gavrovo-Tripolitza and Ionion units. Around 14 Ma oceanic crust of the Mediterranean Ocean arrived at the trench and continued to be subducted until the present-day.

These complex tectonic circumstances have produced many different views on the origin of magmatism in the Aegean Sea/Western Anatolian region. Five groups of models have been suggested for volcanics of the Aegean Sea and Western Anatolia: (1) melting of enriched lithosphere after continent-continent collisions; (2) melting of underplated mafic crust induced by upwelling asthenosphere (e.g. Pe-Piper et al., 2009); (3) decompressional melting due to extension (e.g. Pe-Piper et al., 2009); (4) melting along the edges of subducted slab tears due to asthenospheric upwelling (e.g. Klaver et al., 2016) (5) melting of the mantle wedge by fluids/melts derived from a subducted slab (e.g. Schaarschmidt et al., 2021). It is not to scope of this paper to discuss these different models, but Fig. 7 suggests that calc-alkaline volcanism in the modern SAVA started when subducted oceanic crust did reach $\sim$ 100 km depth underneath the SAVA. If this interpretation is correct, oceanic crust did arrive around 4–5 Ma at 100 km depth at the Sousaki-VF and Aegina-Poros-Methana VF and around 3.0–3.5 Ma at Milos VF, Christiani-Santorini-Kolombo VF and Kos-Nisyros-Yali VF. This observation fits with recent tectonic models (e.g. van Hinsbergen et al., 2020).

Volcanism in the period 5–10 Ma, preceding the development of the modern SAVA, is characterised by calc-alkaline and Na alkaline magmatism of Patmos and the intrusion of granites of Serifos and Lavrion. Subduction of continental crust resulted in slab tears through which magma with an asthenospheric affinity could move upwards and melt adiabatically. Patmos Na-rich volcanism has been interpreted as a result of the interaction between upwelling asthenospheric mantle through a slab tear and interaction with the overlying plate, resulting in intermediate to rhyolitic magmas (e.g. Boehm et al., 2023). Similar underplating of mafic magmas beneath the lower continental crust resulted in melting and intrusion of granites of Serifos and Lavrion that were emplaced in the Aegean upper continental crust (see Fig. 7). In addition, the subduction velocity increased from 5–12 to 35 mm yr^{-1} around the time that volcanism started in the west SAVA section (S-VF and APM-VF).

In summary, this study shows that volcanism in the CSK-VF of the SAVA started around 3 Ma, similar to the Milos and KNY VF and approximately 1–2 Ma later than for the western centres (S-VF and APM-VF). This coincides with the inferred arrival of oceanic crust and accompanying dehydration melting underneath the SAVA VFs and the increase in subduction velocity from 5–12 to 35 mm yr^{-1}.

6 Conclusions

In conclusion the following four statements can be made:

1. Six subaerial samples of the Upper Lava formation from Christiani Island do have a significantly older $^{40}Ar/^{39}Ar$ ages (average 2.56 ± 0.17 Ma (1 sd)) than was previously assumed. Five of the ages are in the time interval of 2.57–2.69 Ma (average 2.63 ± 0.05 Ma, 1 sd), one sample is significantly younger: 2.2 Ma (CH18-02). Sample CH18-14A has a very young age of 133 ka and is most likely derived from a volcanic eruption of Santorini (Middle Pumice Plinian eruption).

2. The volcanic activity of Christiana volcano overlaps with those of other VF of the SAVA. It was contemporary with the youngest intrusions of Sousaki and with Aegina and Methana in the west. Christiana's volcanic activity overlaps with the low volcanic output of Period I of Milos, and with the oldest know volcanic deposit of the KNY volcanic field, the Kefalos dacite of Kos.

3. These new ages for lavas from the Christiano volcano do show that the SAVA was active in all VF around 3.0 Ma and that all the VFs experience periods of quiescence and low volcanic output in the period of 2.0–1.0 Ma.

4. The Christiana volcano was active during NNE-SSW extension, before the stress field changed to NW-SE extension that formed the younger volcanic centres of the CSK volcanic field and the CSK graben.

Code availability. The following software code was used: Koppers (2002).

Data availability. All data is available in Table 1 and in the Supplement.

Supplement. The supplement related to this article is available online at https://doi.org/10.5194/gchron-8-279-2026-supplement.

Author contributions. PZV, XZ and PN collected the samples and did the first selection of suitable samples for Ar/Ar dating. TB prepared the samples for Ar/Ar dating and did the petrography and XRF analyses, KFK and JRW carried out the Ar/Ar dating and interpretation. PZV and TB wrote the manuscript with contributions from all co-authors.

Competing interests. The contact author has declared that none of the authors has any competing interests.

Disclaimer. Publisher's note: Copernicus Publications remains neutral with regard to jurisdictional claims made in the text, published maps, institutional affiliations, or any other geographical representation in this paper. The authors bear the ultimate responsibility for providing appropriate place names. Views expressed in the text are those of the authors and do not necessarily reflect the views of the publisher.

Acknowledgements. We would like to thank Manolis Nomikos for bringing us to Christiani island with a zodiac and Roel van Elsas with the assistance of rock crushing and mineral separation. Marjolein Daeter and Onno Postma did help with the $^{40}Ar/^{39}Ar$ dating. We thank Su-Chin Chang, Tim Druitt and the associate editor Fred Jourdan for the constructive suggestions to improve this paper.

Financial support. Xiaolong Zhou would like to acknowledge grant no. 201506400055 from the China Scholarship Council (CSC). The $^{40}Ar/^{39}Ar$ facility of the VU is covered by NWO grant 834.09.004. This research benefitted from funding from the European Research Council under the European Union's Seventh Framework Programme (FP7/2007-2013)/ERC grant agreement no. 319209. (submitted version).

Review statement. This paper was edited by Fred Jourdan and reviewed by Su-Chin Chang and Tim Druitt.

References

Aarburg, S. and Frechen, M.: Die pyroklastischen Abfolgen der Christiana-lnseln (SüdÄgäis, Griechenland), in: Terrestrische Quartärgeologie, edited by: Becker-Haumann, R., Logabook, Köln, 260–276, ISBN 3-934346-03-0, 1999.

Allen, S. R.: Reconstruction of a major caldera-forming eruption from pyroclastic deposit characteristics: Kos Plateau Tuff, eastern Aegean Sea, J. Volcanol. Geoth. Res., 105, 141–162, https://doi.org/10.1016/S0377-0273(00)00222-5, 2001.

Altunkaynak, S., Dilek, Y., Cenc, C. S., Sunal, G., Gertisser, R., Furnes, H., Foland, K. A., and Yang, J.: Spatial, temporal and geochemical evolution of Oligo-Miocene granitoid magmatism in western Anatolia, Turkey, Gondwana Res., 21, 961–986, https://doi.org/10.1016/j.gr.2011.10.010, 2012.

Bachmann, O., Schoene, B., Schnyder, C., and Spikings, R.: $^{40}Ar/^{39}Ar$ and U/Pb dating of young rhyolites in the Kos-Nisyros volcanic complex, Eastern Aegean Arc (Greece): age discordance due to excess ^{40}Ar in biotite, Geochem. Geophy. Geosy., 11, Q0AA08, https://doi.org/10.1029/2010GC003073, 2010.

Bailey, J., Jensen, E., Hansen, A., Kann, A., and Kann, K.: Formation of heterogeneous magmatic series beneath North Santorini, South Aegean island arc, Lithos, 110, 20–36, https://doi.org/10.1016/j.lithos.2008.12.002, 2009.

Boehm, K. M., Kuiper, K. F., Uzel, B., Vroon, P. Z., and Wijbrans, J. R.: Volcanism straddling the Miocene–Pliocene boundary on Patmos and Chiliomodi islands (southeastern Aegean Sea): insights from new $^{40}Ar/^{39}Ar$ ages, Geochronology, 5, 391–403, https://doi.org/10.5194/gchron-5-391-2023, 2023.

Branca, S., Coltelli, M., De Beni, E., and Wijbrans, J.: Geological evolution of Mount Etna volcano (Italy) from earliest products until the first central volcanism (between 500 and 100 ka ago) inferred from geochronological and stratigraphic data, Int. J. Earth Sci., 97, 135–152, https://doi.org/10.1007/s00531-006-0152-0, 2008.

Brun, J. P. and Sokoutis, D.: 45 Myr of Aegean crust and mantle flow driven by trench retreat, Geology, 38, 815–818, https://doi.org/10.1130/G30950.1, 2010.

Castellanos Melendez, M. P., di Muro, A., Laurent, O., Kuiper, K., Wijbrans, J. R., and Bachmann, O.: Explosive volcanism of Piton des Neiges (Reunion Island) and excess age dispersion in sanidine: Insights into magma chamber processes in a hotspot setting, Chem. Geol., 632, 121539, https://doi.org/10.1016/J.CHEMGEO.2023.121539, 2023.

Dietrich, V. J. and Lagios, E.: Nisyros Volcano: The Kos-Yali-Nisyros Volcanic Field, Springer, https://doi.org/10.1007/978-3-319-55460-0, 2017.

Druitt, T., Kutterolf, S., Ronge, T. A., Hübscher, C., Nomikou, P., Preine, J., Gertisser, R., Karstens ,J., Keller, J., Koukousioura, O., Manga, M., Metcalfe, A., McCanta, M., McIntosh, I., Pank, K., Woodhouse, A., Beethe, S., Berthod, C., Chiyonobu, S., Chen, H., Clark, A., DeBari, S., Johnston, R., Peccia, A., Yamamoto, Y., Bernard, A., Fernandez Perez, T., Jones, C., Batuk Joshi, K., Kletetschka, G., Li, X., Morris, A., Polymenakou, P., Tominaga, M., Papanikolaou, D., Wang K.-L., and Lee, H.-Y.: Giant offshore pumice deposit records a shallow submarine explosive eruption of ancestral Santorini, Commun. Earth Environ., 5, 24, https://doi.org/10.1038/s43247-023-01171-z, 2024.

Druitt, T. H., Edwards, L., Mellors, R. M., Sparks, R. S. J., Lanphere, M., Davies, M., and Barreirio, B.: Santorini Volcano, Geological Society of London, 19, https://doi.org/10.1144/GSL.MEM.1999.019.01.12, 1999.

Druitt, T. H., McCoy, F. W., and Vougioukalakis, G. E.: The Late Bronze Age eruption of Santorini Volcano and its impact on the Ancient Mediterranean World, Elements, 15, 185–190, https://doi.org/10.2138/gselements.15.3.185, 2019.

Elburg, M., Smet, I., Van den Haute, P., Vanhaecke, F., Klaver, M., and Andersen, T.: Extreme isotopic variation documents extensional tectonics in arc magmas from Methana, Greece, Lithos, 318–319, 386–398, https://doi.org/10.1016/j.lithos.2018.08.029, 2018.

Ersoy, E. Y. and Palmer, M. R.: Eocene-Quaternary magmatic activity in the Aegean: Implications for mantle metasomatism and magma genesis in an evolving orogeny, Lithos, 180, 5–24, https://doi.org/10.1016/j.lithos.2013.06.007, 2013.

Francalanci, L., Vougioukalakis, G. E., Perini, G., and Manetti, P.: A West-East Traverse along the magmatism of the south Aegean volcanic arc in the light of volcanological, chemical and isotope data, Dev. Volcano., 7, 65–111, https://doi.org/10.1016/S1871-644X(05)80033-6, 2005.

Heath, B. A., Hooft, E. E. E., Toomey, D. R., Papazachos, C. B., Nomikou, P., Paulatto, M., Morgan, J. V., and Warner, M. R.: Tectonism and Its Relation to Magmatism Around Santorini Volcano From Upper Crustal P Wave Velocity, J. Geophys. Res.-Sol. Ea., 124, 10610–10629, https://doi.org/10.1029/2019JB017699, 2019.

Heath, M., Phillips, D., and Matchan, E. L.: An evidence-based approach to accurate interpretation of 40Ar/39Ar ages from basaltic rocks, Earth Planet. Sc. Lett., 498, https://doi.org/10.1016/j.epsl.2018.06.024, 65–76, 2018.

Hübscher, C., Ruhnau, M., and Nomikou, P.: Volcano-tectonic evolution of the polygenetic Kolumbo submarine volcano/Santorini (Aegean Sea), J. Volcanol. Geoth. Res., 291, 101–111, https://doi.org/10.1016/j.jvolgeores.2014.12.020, 2015.

IJlst, L.: A laboratory overflow-centrifuge for heavy liquid mineral separation, Am. Mineral., 58, 1088–1093, 1973.

Jolivet, L. and Brun, J. P.: Cenozoic geodynamic evolution of the Aegean, Int. J. Earth Sci., 99, 109–138, https://doi.org/10.1007/s00531-008-0366-4, 2010.

Jolivet, L., Faccenna, C., Huet, B., Labrousse, L., Le Pourhiet, L., Lacombe, O., Lecomte, E., Burov, E., Denèle, Y., Brun, J., Philippon, M., Paul, A., Salaün, G., Karabulut, H., Piromallo, C., Monié, P., Gueydan, F., Okay, A., Oberhänsli, R., Pourteau, A., Augier, R., Gadenne, L., and Driussi, O.: Aegean tectonics: Strain localisation, slab tearing and trench retreat, Tectonophysics, 597–598, 1–33, https://doi.org/10.1016/j.tecto.2012.06.011, 2013.

Karstens, J., Preine, J., Crutchley, G. J., Kutterolf, S., van der Bilt, W. G. M., Hooft, E. E. E., Druitt, T. H., Schmid, F., Magne Cederstrøm, J., Hübscher, C., Nomikou, P., Carey, S., Kühn, M., Judith Elger, J., and Berndt, C.: Revised Minoan eruption volume as benchmark for large volcanic eruptions, Nat. Commun., 14, 2497, https://doi.org/10.1038/s41467-023-38176-3, 2023.

Keller, J., Volker, D., Reusser, E., Gertisser, R., and Aarburg, S.: Recognition of a major ignimbrite in the early evolution of the Santorini Group: the Christiani Ignimbrite, Conference Cities on Volcanoes 6, 2010, https://www.earth-prints.org/bitstream/2122/6924/1/CitiesonVolcanoes6AbstractsVolume.pdf (last access: 18 December 2024, no longer available online), 2010.

Keller, J., Gertisser, R., Reusser, E., and Dietrich, V.: Pumice deposits of the Santorini Lower Pumice 2 eruption on Anafi island, Greece: Indications for a Plinian event of exceptional magnitude, J. Volcanol. Geoth. Res., 278, 120–128, https://doi.org/10.1016/j.jvolgeores.2014.04.009, 2014.

Klaver, M.: Dynamics of magma generation and differentiation in the central-eastern Aegean arc: A geochemical and petrological study of Quaternary arc volcanism in Greece, PhD thesis, Vrije Universiteit Amsterdam, 213 pp., ISBN 978-94-623-3292-8, https://research.vu.nl/en/publications/dynamics-of-magma-generation-and-differentiation-in-the-central-e/ (last access: 30 April 2026), 2016.

Koppers, A.: ArArCALC software for $^{40}Ar/^{39}Ar$ age calculationsl, Comput. Geosci., 28, 605–619, https://doi.org/10.1016/S0098-3004(01)00095-4, 2002.

Kuiper, K., Deino, A., Hilgen, F., Krijgsman, W., Renne, P., and Wijbrans, J.: Synchronizing Rock Clocks of Earth History, Science, 320, 500–504, https://doi.org/10.1126/science.1154339, 2008.

Lee, J., Marti, K., Severinghaus, J., Kawamura, K., Yoo, H., Lee, J., and Kim, J.: A redetermination of the isotopic abundances of atmospheric Ar, Geochim. Cosmochim. Ac., 70, 4507–4512, https://doi.org/10.1016/j.gca.2006.06.1563, 2006.

Le Pichon, X., Lallemant, S. J., Chamot-Rooke, N., Lemeur, D., and Pascal, G.: The Mediterranean Ridge backstop and the Hellenic nappes, Mar. Geol., 186, 111–125, https://doi.org/10.1016/S0025-3227(02)00175-5, 2002.

Metcalfe, A., Druitt, T., Pank, K., Kutterolf, S., Preine, J., Beethe, S., Schmitt, A., Hübscher, C., Nomikou, P., Ronge, T.A., Berthod, C., Chen, H., Chiyonobu, S., Clark, A., DeBari, S., Gertisser, R., Johnston, R., Koukousioura, O., Manga, M., McCanta, M., McIntosh, I., Peccia, A., Tominaga, M., Yamamoto, Y., Woodhouse, A., Bernard, A., Fernandez Perez, T., Jones, C.K., Batuk Joshi, K., Kletetschka, G., Morris, A., Polymenakou, P., Li, X., Papanikolaou, D., Pyle, D., and Sternai, P.: Tectonic modulation of caldera volcanism on the South Aegean Volcanic Arc, Earth Planet. Sc. Lett., 671, 119633, https://doi.org/10.1016/j.epsl.2025.119633, 2025.

Min, K., Mundil, R., Renne, P., and Ludwig, K.: A test for systematic errors in $^{40}Ar/^{39}Ar$ geochronology through comparison with U/Pb analysis of a 1.1-Ga rhyolite, Geochim. Cosmochim. Ac., 64, 73–98, https://doi.org/10.1016/S0016-7037(99)00204-5, 2000.

Mountrakis, D. M., Pavlidis, S., Chatzipetros, A., Meletlidus, S., Tranos, M. D., Vougioukalakis, G. E., and Killias, A.: Active deformation of Santorini, Proceedings of the Second Workshop Santorini, Greece, 2–4 May 1996, EUR18161 – The European laboratory volcanos, edited by: Casale, R., Fytikas, M., Sigvaldasson, G., and Vougioukalakis, G., Official Publications of the European Communities, Luxembourg [European Commision], 13–22, 1996.

Nomikou, P., Papanikolaou, D., Alexandri, M., Sakellariou, D., and Rousakis, G.: Submarine volcanoes along the Aegean volcanic arc, Tectonophysics, 597–598, 123–146, https://doi.org/10.1016/j.tecto.2012.10.001, 2013.

Nomikou, P., Hübscher, C., and Carey, S.: The Christiana–Santorini–Kolumbo Volcanic Field, Elements, 15, 171–176, https://doi.org/10.2138/gselements.15.3.171, 2019.

Pe-Piper, G. and Piper, D.: The effect of changing regional tectonics on an arc volcano: Methana, Greece, J. Volcanol. Geoth. Res., 260, 146–163, https://doi.org/10.1016/j.jvolgeores.2013.05.011, 2013.

Pe-Piper, G., Piper, D. J. W., Koukouvelas, I., Dolansky, L. M., and Kokkals, S.: Postorogenic shoshonitic rocks and their origin by melting underplated basalts: The Miocene of Limnos, Greece, GSA Bulletin, 121, 39054, https://doi.org/10.1130/B26317.1, 2009.

Piper, D., Pe-Piper, G., Perissoratis, C., and Anastasakis, G.: Distribution and chronology of submarine volcanic rocks around Santorini and their relationship to faulting, Geological Society, London, Special Publications, 29, 99–111, https://doi.org/10.1144/SP291.5, 2007.

Piper, D., Pe-Piper, G., Anastasakis, G., and Reith, W.: The volcanic history of Pyrgousa – volcanism before the eruption of the Kos Plateau Tuff, B. Volcanol., 81, 32, https://doi.org/10.1007/s00445-019-1290-0, 2019.

Popa, R. G., Guillong, M., Bachmann, O., Szymanowski, D., and Ellis, B.: U-Th zircon dating reveals a correlation between eruptive styles and repose periods at the Nisyros-Yali volcanic area, Greece, Chem. Geol., 555, 119830, https://doi.org/10.1016/j.chemgeo.2020.119830, 2020.

Preine, J., Karstens, J., Hübscher, C., Nomikou, P., Schmid, F., Crutchley, G. J., Druitt, T. H., and Papanikolaou, D.: Spatio-temporal evolution of the Christiana-Santorini-Kolumbo volcanic field, Aegean Sea, Geology, 50, 96–100, https://doi.org/10.1130/G49167.1, 2021.

Preine, J., Hübscher, C., Karstens, J., and Nomikou, P.: Volcano-tectonic evolution of the Christiana-Santorini-Kolumbo rift zone, Tectonics, 41, e2022TC007524, https://doi.org/10.1029/2022TC007524, 2022a.

Preine, J., Karstens, J., Hübscher, C., Crutchley, G. J., Schmid, F., Crutchley, G. J., Druitt, T. H., Schmid, F., and Nomikou, P.: The Hidden Giant: How a rift pulse triggered a cascade of sector collapses and voluminous secondary mass-transport events in the early evolution of Santorini, Basin Res., 34, 1465–1485, https://doi.org/10.1111/bre.12667, 2022b.

Puchelt, H., Murad, E., and Hubberten, H.-W.: Geochemical and petrological studies of lavas, pyroclastica and associated xenoliths from the Christiana Islands, Aegean Sea, Neues Jb. Miner. Abh., 131, 140–155, 1977.

Ring, U., Glodny, J., Will, T., and Thomson, S. N.: The Hellenic subduction system: High-pressure metamorphism, exhumation, normal faulting, and large-scale extension, Annu. Rev. Earth Pl. Sc., 38, 45–76, https://doi.org/10.1146/annurev.earth.050708.170910, 2010.

Schaarschmidt, A., Haase, K. M., Voudouris, P. C., Melfos, V., and Klemd, R.: Migration of Arc Magmatism Above Mantle Wedge Diapirs With Variable Sediment Contribution in the Aegean, Geochem. Geophy. Geosy., 22, e2020GC009565, https://doi.org/10.1029/2020GC009565, 2021.

Schaen, A. J., Jicha, B. R., Hodges, K. V., Vermeesch, P., Stelten, M. E., Mercer, C. M., Phillips, D., Rivera, T. A., Jourdan, F., Matchan, E. L., Hemming, S. R., Morgan, L. E., Kelley, S. P., Cassata, W. S., Heizler, M. T., Vasconcelos, P. M., Jeff, A. Benowitz, J. A., Koppers, A. A. P., Mark, D. F., Niespolo, E. M., Sprain, C. J., Hames, W. E., Kuiper, K. F., Turrin, B. D., Renne, P. R., Ross, J., Nomade, S., Guillou, H., Webb, L. E., Cohen, B. A., Calvert, A. T., Joyce, N., Ganerød, M., Wijbrans, J., Ishizuka, O., He, H., Ramirez, A., Pfänder, J. A., Lopez-Martínez, M., Qiu, H., and Singer, B. S.: Interpreting and reporting $^{40}Ar/^{39}Ar$ geochronologic data, GSA Bulletin, 133, 461–487, https://doi.org/10.1130/B35560.1, 2021.

Smith, P. E., York, D., Chen, Y., and Evensen, N. M.: Single crystal ^{40}Ar-^{39}Ar dating of a Late Quaternary paroxysm on Kos, Greece: Concordance of terrestrial and marine ages, Geophys. Res. Lett., 23, 3047–3050, https://doi.org/10.1029/96GL02759, 1996.

Spakman, W., Wortel, M. J. R., and Vlaar, J. N.: The Hellenic Subduction Zone: A tomographic image and its geodynamic implications, Geophys. Res. Lett., 15, 60–63, https://doi.org/10.1029/GL015i001p00060, 1988.

van Hinsbergen, D. J., Vissers, R. L., and Spakman, W.: Origin and consequences of western Mediterranean subduction, rollback, and slab segmentation, Tectonics, 33, 393–419, https://doi.org/10.1002/2013TC003349, 2014.

van Hinsbergen, D. J. J., Torsvik, T. H., Schmid, S. M., Maţenco, L. C., Maffione, M., Vissers, R. L. M., Gürer, D., and Spakman, W.: Orogenic architecture of the Mediterranean region and kinematic reconstruction of its tectonic evolution since the Triassic, Gondwana Res., 81, 79–229, https://doi.org/10.1016/j.gr.2019.07.009, 2020.

Vougioukalakis, G., Satow, C., and Druitt, T.: Volcanism of the South Aegean Volcanic Arc, Elements, 15, 159–164, https://doi.org/10.2138/gselements.15.3.159, 2019.

Wei, W., Zhai, D., Wei, F., Bai, X., and Xu, J.: Mantle Dynamics of the Eastern Mediterranean and Middle East: Constraints From P-Wave Anisotropic Tomography, Geochem. Geophy. Geosy., 20, 4505–4530, https://doi.org/10.1029/2019GC008512, 2019.

Wortel, M. J. R. and Spakman, W.: Subduction and Slab Detachment in the Mediterranean-Carpathian Region, Science, 290, 1910–1917, https://doi.org/10.1126/science.290.5498.1910, 2000.

Zhou, X., Kuiper, K., Wijbrans, J., Boehm, K., and Vroon, P.: Eruptive history and $^{40}Ar/^{39}Ar$ geochronology of the Milos volcanic field, Greece, Geochronology, 3, 273–297, https://doi.org/10.5194/gchron-3-273-2021, 2021.